metals

MDPI

Article

Influence of Mo Content on the Precipitation Behavior of 13Ni Maraging Ultra-High Strength Steels

Daniela P. M. da Fonseca [1,*], Maria Virginia P. Altoé [2], Braulio S. Archanjo [3], Emilia Annese [4] and Angelo F. Padilha [5]

1 Instituto SENAI de Inovação em Sistemas de Manufatura e Processamento a Laser, Joinville 89218-153, SC, Brazil
2 Molecular Foundry, Lawrence Berkeley National Laboratory (LBNL), Berkeley 94720, CA, USA; mvpaltoe@lbl.gov
3 Divisão de Metrologia de Materiais, Instituto Nacional de Metrologia, Qualidade e Tecnologia (Inmetro), Duque de Caxias 25250-020, RJ, Brazil; bsarchanjo@inmetro.gov.br
4 Brazilian Center for Physics Research, Rio de Janeiro 22290-180, RJ, Brazil; emilia.annese@gmail.com
5 Departamento de Engenharia Metalúrgica e de Materiais, Escola Politécnica da Universidade de São Paulo (EP-USP), São Paulo 05508-030, SP, Brazil; padilha@usp.br
* Correspondence: danipassarelo@alumni.usp.br

Abstract: This study offers valuable insights into the precipitation behavior of 13Ni maraging steels, emphasizing the role of molybdenum content in their microstructure, strengthening, and precipitate evolution. Precipitate morphology and crystallography were examined using a combination of high-resolution transmission electron microscopy and selected area electron diffraction. Strengthening mechanisms were assessed through Vickers hardness measurements. All the examined samples exhibited a lath martensite microstructure and displayed an increasing hardness over the aging time. The molybdenum content not only influenced the presence of retained austenite in the initial microstructure but also affected the type of precipitates formed during the early aging stages. Initially, Ni_3Mo precipitates were formed, succeeded by the formation of more stable Fe_2(Mo,Ti) Laves precipitates. The ultra-high strength of 13Ni maraging steels arises from the combination of the precipitate type and size distribution. The base composition of 13Ni maraging steels achieved a peak hardness of 798 HV1 through the precipitation of Laves Fe_2(Mo,Ti) phases ranging from 3 to 14 nm in diameter.

Keywords: 13Ni maraging steels; molybdenum; precipitation hardening; precipitates; strengthening

check for updates

Citation: da Fonseca, D.P.M.; Altoé, M.V.P.; Archanjo, B.S.; Annese, E.; Padilha, A.F. Influence of Mo Content on the Precipitation Behavior of 13Ni Maraging Ultra-High Strength Steels. *Metals* **2023**, *13*, 1929. https://doi.org/10.3390/met13121929

Academic Editor: Andrii Kostryzhev

Received: 17 October 2023
Revised: 14 November 2023
Accepted: 21 November 2023
Published: 24 November 2023

Copyright: © 2023 by the authors. Licensee MDPI, Basel, Switzerland. This article is an open access article distributed under the terms and conditions of the Creative Commons Attribution (CC BY) license (https://creativecommons.org/licenses/by/4.0/).

1. Introduction

Maraging steels are among the highest strength steels commercially available. They have extremely low carbon content, and after being air-cooled from the austenitic phase, they exhibit a ductile and tough non-twinned martensite structure in the form of packets and laths, with a high density of dislocations. The significant increase in strength is attributed to precipitation hardening, which occurs due to the formation of nanometric intermetallic particles during the subsequent aging of the martensite ("maraging") in the temperature range of 400 to 600 °C [1–3].

Studies on maraging steels (Fe–Ni–Co–Mo) have reported several possible types of precipitates, including Ni_3Mo, Ni_3Ti, Laves Fe_2Mo, Laves Fe_2Ti, σ–FeMo, σ–FeTi, and μ–Fe_7Mo_6. These precipitates can exhibit spherical or elongated (needle or rod-like) shapes. Typically, their dimensions range from 5 to 20 nm, with distances between precipitates of approximately 100 nm [4,5].

The most conventional and widely used commercially is the 18Ni maraging steel, which consists of Fe–18Ni–(8–9)Co–(3–5)Mo–(<1)Ti (wt.%) and has a yield strength of approximately 1.7 GPa. Our study was about 13Ni maraging steel, an ultra-high-strength maraging

steel with a base composition of Fe–13Ni–15Co–10Mo–1Ti (wt.%), also known as maraging 400, and it can achieve a yield strength of 3 GPa (as reported in the literature) [1,6–9]. The primary approach used to achieve these high mechanical strength values in 13Ni maraging steels is the increase in the volume fraction of precipitates, thereby enhancing the hardening effect through higher molybdenum and titanium contents in the steel [3,4,9–15]. Molybdenum directly participates in the formation of precipitates, while cobalt synergistically reduces the solubility of molybdenum in the matrix [4,16,17]. However, due to molybdenum's role as an austenite stabilizer, it is necessary to reduce the nickel content to maintain the steel in the martensitic phase [4,18].

Fukamachi et al. conducted a detailed study using electron diffraction in a transmission electron microscope to identify the precipitates formed during the aging process of a maraging steel with the composition Fe–13.01Ni–15.30Co–9.83Mo–0.24Ti (wt.%) at three different temperatures: 450 °C, 500 °C, and 550 °C [19]. Their findings revealed the presence of two types of precipitates within the martensitic matrix: Ni_3Mo and Fe_2Mo. Initially, Ni_3Mo precipitation occurs, and at the peak hardness observed at the three temperatures, both Ni_3Mo and Fe_2Mo precipitates are present. Generally, it can be concluded that the Laves Fe_2Mo phase precipitates at higher temperatures and/or for longer durations than the Ni_3Mo compound [9,19]. The average size of the precipitates at the peak hardness was approximately 5 nm [19].

In a more recent study by Niu et al., ultra-high-strength maraging steels with a composition of Fe–17.7Ni–15.0Co–6.6Mo–1.0Ti (wt.%) (yield strength of 2.5 GPa) were investigated using TEM (Transmission Electron Microscopy), APT (Atom Probe Tomography), and mechanical testing [8]. The study revealed the initial Ni_3Ti type in these steels. These precipitates originate from nickel and titanium-rich clusters, which were detected by APT within the first 15 min of aging at 480 °C. The precipitates exhibit an elongated (needle-like) morphology with dimensions ranging from 3 to 8 nm. For longer aging times, starting from 4 h, a molybdenum-rich phase nucleates at the interface between the Ni_3Ti precipitates and the matrix. This molybdenum-rich phase forms a core–shell structure that encapsulates the Ni_3Ti phase, preventing its growth [8]. Similarly, Tian et al. also observed this core–shell structure under similar conditions in Fe–13.0Cr–7.5Ni–7.0Co–3.0Mo–1.7Ti (wt.%) maraging steels [17].

In a subsequent study, Niu et al. investigated three Fe–13Cr–7Ni–7Co alloys with varying molybdenum and titanium content (3 wt.%Mo and 0 wt.%Ti, 0 wt.%Mo and 1 wt.%Ti, 3 wt.%Mo and 1 wt.%Ti) at peak hardness [16]. Their observations revealed that increasing the molybdenum content resulted in faster precipitation kinetics of Ni_3Ti and a higher precipitate density. They stated a synergistic effect between molybdenum and titanium, where alloys containing both 3 wt.%Mo and 1 wt.%Ti exhibited finer molybdenum-rich precipitates compared to the alloy containing only 3 wt.%Mo (without titanium additions) [16].

Overall, among the molybdenum-rich intermetallic precipitates, the most commonly reported type in 13Ni maraging steels is Ni_3Mo. It exhibits an orthorhombic structure and can have either a rod-like or spherical morphology. However, there is no consensus in the published literature about the structure or morphology. The dimensions of Ni_3Mo precipitates are approximately 0.25 nm × 50 nm at the peak hardness. Previous works [4,20] have suggested that Ni_3Mo precipitates are metastable, and when subjected to long aging times and/or temperatures above 480 °C, they can be replaced by Fe_2Mo or σ–FeMo precipitates. This transformation is particularly observed in alloys with higher molybdenum contents and/or lower nickel contents. Initially, the improved lattice fit between Ni_3Mo and the matrix favors the precipitation of this metastable compound. However, its growth is limited by the increased coherence stresses, promoting the formation of equilibrium precipitates that nucleate at the interface between Ni_3Mo and the matrix. These molybdenum-rich precipitates can also be identified as Fe_2Mo or μ–Fe_7Mo_6 [4,6–8,20,21]. Regarding titanium-rich precipitates, the most commonly reported compound is Ni_3Ti, particularly in alloys with higher titanium contents. This compound often combines with molybdenum to form Ni_3(Mo,Ti) precipitates [4,5,21–23].

The 13Ni maraging steels have a lower fracture toughness than 18Ni (300) maraging steels, around 60% lower. Because of this, over the years, studies on the precipitation of this system have focused more on 18Ni maraging steels. The most recent works, using advanced microstructural characterization techniques, which have added a lot to the understanding of these precipitates, were carried out for 18Ni maraging steels and other unconventional maraging steels still with a high nickel content. However, the literature has shown that changes in the alloy composition lead to significant variations in the microstructure of the precipitates, affecting their type, morphology, and interaction with one another [16].

This highlights the existence of a knowledge gap to be filled in the field of physical metallurgy concerning these 13Ni maraging steels. Few studies have attempted to characterize the precipitates in 13Ni maraging steels, primarily because these precipitates are even smaller compared to other maraging steels, making their characterization a challenging task. With the advent of high-resolution characterization techniques, the investigation of this material is feasible and paving the way for new insights about the issue. Therefore, the development of novel heat treatment methods, enhancements in mechanical properties, and the exploration of new industrial applications have been studied.

In the aforementioned context, our research focuses on conducting experimental studies using High-Resolution Transmission Electron Microscopy (HRTEM) and Selected Area Electron Diffraction (SAED) to investigate the phase transformations in solid-state 13Ni maraging steels. The objective was to understand the influence of alloying elements, mainly molybdenum, on the phase transformation of precipitates and on the precipitation hardening mechanisms of 13Ni maraging steels.

2. Materials and Methods

A non-commercial 13Ni maraging steel (MS) was produced through vacuum induction melting (VIM) and electroslag remelting (ESR). Subsequently, the ingot was homogenized at 1250 °C for 5 h, forged, and hot rolled. Three different compositions were produced: low Mo content (MS1), base composition (MS2), and high Mo content (MS3)—as shown in Table 1. The samples were cut, packed in stainless steel foil to minimize oxidation, solution annealed (AN) at 1200 °C for 1 h, and quenched in water to ensure a fully martensitic structure. Finally, the samples were aged (AG) at 480 °C for 3–6 h. The temperature and time were selected based on previous studies in the literature, which identified this combination as the optimal regime for studying precipitation at peak hardness. After the aging treatment, the samples were polished and etched with Vilella's reagent (1 g picric acid, 5 mL HCl, and 100 mL ethanol). The microstructures of the samples under different conditions were observed using Optical Microscopy (OM) and Focused Ion Beam with Ion Channeling Contrast (FIB/iCC) (FEIDualBeam Helios NanoLab 650, Duque de Caxias, Brazil). Vickers hardness measurements were made using a load of 1 kg for 15 s. TEM specimens were prepared using a Focused Ion Beam (FIB) (FEI DualBeam Helios NanoLab 650, Duque de Caxias, Brazil) and characterized using a Transmission Electron Microscope (TEM) (JEOL 2100F, Berkeley, CA, USA), operated at 200 kV. The phases identified were indexed by calculating the interplanar distance and using the ICSD files: martensite 64795, austenite 44862, Fe_2Mo 632626, Fe_2Ti 107646, Ni_3Mo 105046 and Ni_3Ti 30216. The identification of the precipitates formed during aging were established by reconciling dark-field Transmission Electron Microscopy (DF-TEM), Selected Area Electron Diffraction (SAED), and High-Resolution Transmission Electron Microscopy (HRTEM) results from samples of MS1 aged for 6 h, non-aged MS2, MS2 aged for 3 h, MS2 aged for 6 h, and MS3 aged for 6 h.

Table 1. Chemical composition of the studied maraging steels (wt.%).

	Fe	Ni	Co	Mo	Ti	Si	Mn
MS1	Bal.	13.40	14.96	7.51	0.250	0.150	0.160
MS2	Bal.	12.85	15.64	10.49	0.721	0.040	0.040
MS3	Bal.	14.06	15.21	15.02	0.240	0.060	0.040

3. Results and Discussion

3.1. Microstructure

Figure 1a depicts a schematic illustration of a typical martensite microstructure characterized by a hierarchical structure of primary austenite grain, packets, blocks, and laths. These structures and morphologies were understood through experimental studies, as will be presented in the results below.

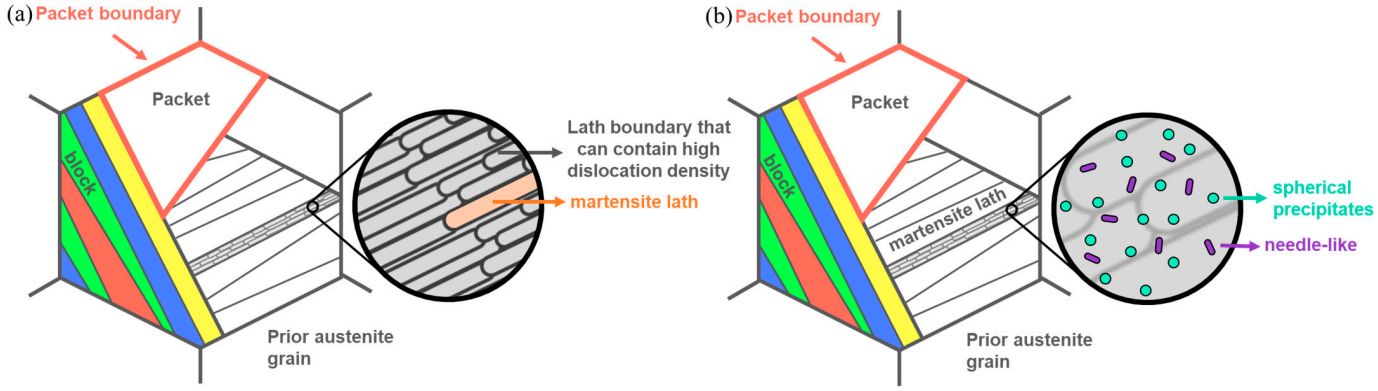


Figure 1. Schematic illustration, exhibiting the morphology of typical microconstituents formed in the maraging steels. (**a**) After annealing, maraging steels have a microstructure with hierarchical structure of primary austenite grain, packets, blocks, and laths. (**b**) After aging, the recovery process of the martensitic matrix and the formation of nanometric precipitates occur, usually presenting a spherical or needle-life morphology.

The characteristic microstructure is due to a sequence of heat treatments that lead to solid-state phase transformations in maraging steels. During the annealing (1200 °C), there is the austenite phase transformation which generates the primary austenite grain [24]. During quenching, via the shear mechanism, the austenite transforms in martensite forming the packet, block, and lath structures [25,26]. The matrix exhibits a high density of dislocations (usually greater than $10^{11–12}$ cm^{-2}) and dislocation tangles, both of which act as nucleation sites for precipitates during the early stages of aging [3,9]. Figure 1b shows the illustration of these precipitates formed during aging, which usually present with spherical or needle-life morphology [21,27]. After aging, the austenite grain size remained the same, while the martensite laths increased in size, and dislocations disappeared with increasing aging time. Some authors suggest that during the early stages of aging, there is typically a decrease in the density of dislocations, along with a rearrangement of the microstructure as part of the martensitic matrix recovery process [4,28].

Figure 2 displays OM images (Figure 2a–c), FIB/iCC images (Figure 2d–f), and bright-field Transmission Electron Microscopy (BF-TEM) images (Figure 2g–i) of the microstructure of samples aged at 480 °C for 6 h. The BF-TEM images are of lamellae obtained from the cross-section of the surface shown in the FIB/iCC images. The images show the characteristic morphology of these steels: primary austenite grain, packets, blocks, and laths. Samples MS1, MS2, and MS3 exhibited primary austenite grains with sizes of 350–450 µm, 250–350 µm, and 200–300 µm, respectively.

In the case of the MS3 sample, certain regions, up to 50 µm, contained retained austenite (RA), as shown in Figure 2g–i (pink arrows) (confirmed through XRD measurements, presented Appendix A). The orientation relationship between martensite and retained austenite followed the Nishiyama–Wassermann (N-W) type, $(\bar{1}\bar{1}1)_{\gamma}//(01\bar{1})_{M,\alpha}$, $[\bar{1}12]_{\gamma}//[011]_{M,\alpha}$, which is commonly observed experimentally [5,22]. Transmission electron microscopy analyses revealed smaller austenite areas within martensite laths, exhibiting spherical morphology with dimensions of approximately 10–25 nm, as well as austenite at the lath boundaries with dimensions of 40–80 nm. Additionally, besides the

retained austenite (RA), sample MS3 exhibited the partial presence of lenticular and thin plate martensite amidst lath martensite, showing less defined packets, thinner blocks, and lower martensite transformation start (Ms) and finishes (Mf) temperatures, similar to the martensitic microstructure of steels containing 0.6–0.8 wt.%C carbon [5,29–31].

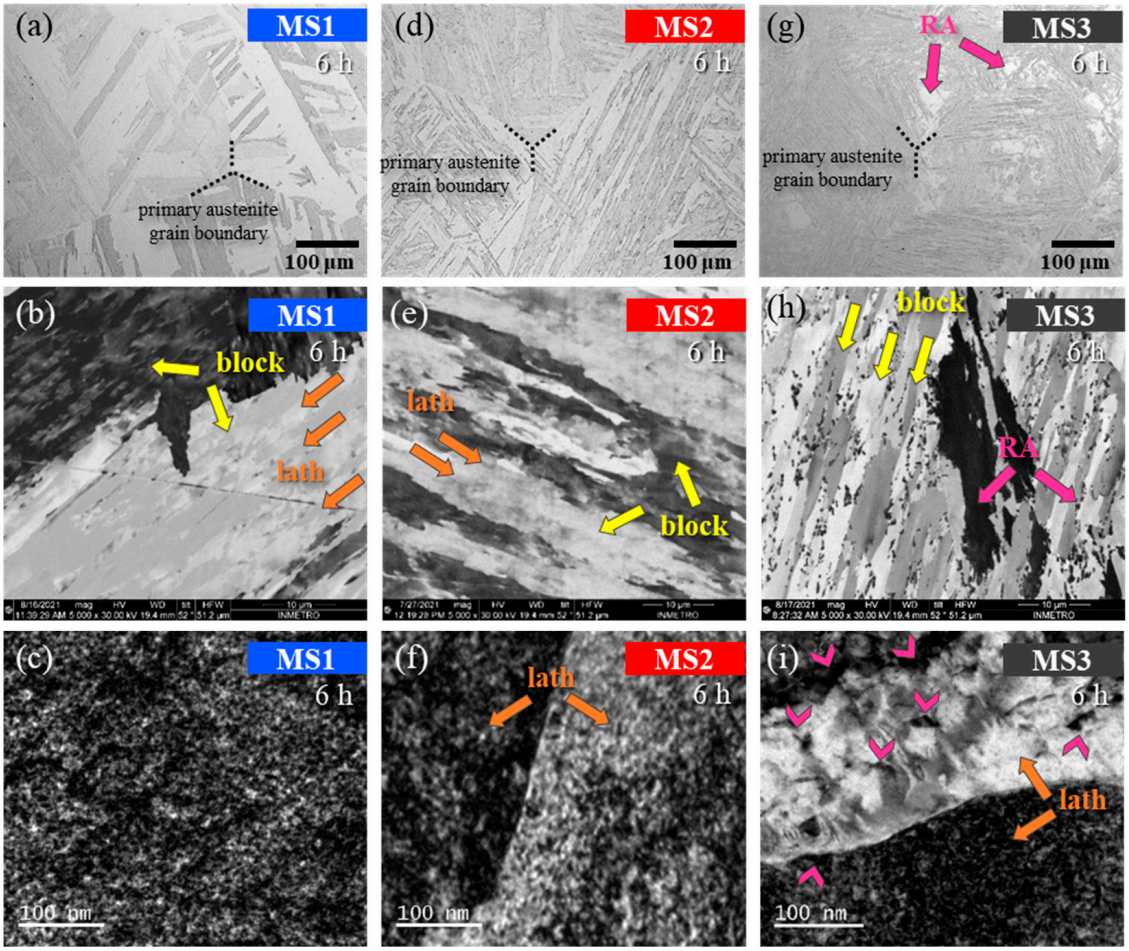


Figure 2. OM, FIB/iCC, and cross-section lamellae BF-TEM images of samples (**a**–**c**) MS1, (**d**–**f**) MS2, and (**g**–**i**) MS3. Aged at 480 °C for 6 h, etched with Vilella's. Dotted lines indicate primary austenite grain boundary, pink arrows show regions with retained austenite (RA), yellow arrows indicate martensite blocks and orange arrows indicate martensite laths.

3.2. Phase Transformation

Figure 3 shows the representative DF-TEM, SAED pattern, HRTEM, and Fast Fourier Transform (FTT) images of the sample MS2 aged at 480 °C for 6 h. The DF-TEM image (from spot $2\bar{1}0$ of the precipitates) displays spherical-shaped precipitates in bright contrast (Figure 3a), distributed throughout the matrix. The SAED pattern and the FTT image confirmed the hexagonal crystal structure of $Fe_2(Mo,Ti)$. The orientation relationship between the $Fe_2(Mo,Ti)$ phase and the martensite matrix was found to be $(01\bar{1})_p//(2\bar{2}1)_M$, $[122]_p//[111]_M$. The precipitates have dimensions of approximately 2 nm × 4 nm and a diffuse precipitate–matrix interface, lacking a well-defined edge (Figure 3b). This analysis was performed on all samples, and the results are compiled in Figure 4 and Table 2. The size classification considered precipitates with an average diameter smaller or equal to 8 nm as "small" and those with an average diameter larger than 8 nm as "large".

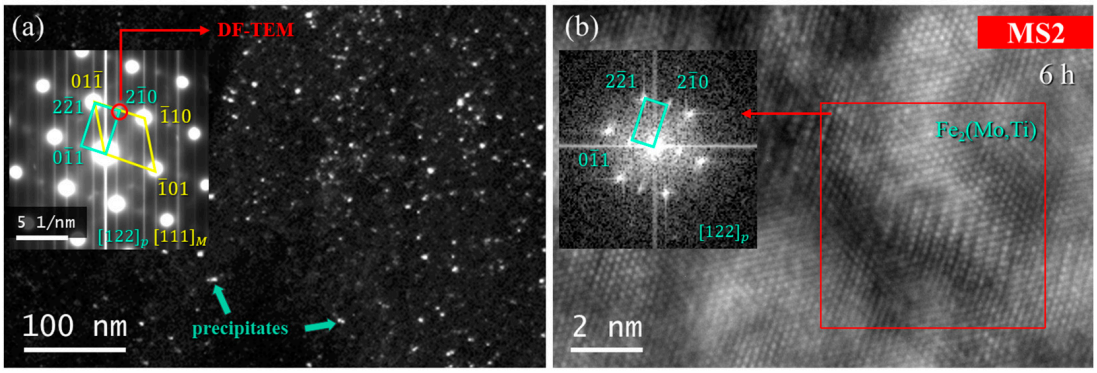


Figure 3. Precipitates $Fe_2(Mo,Ti)$ in bright contrast distributed throughout the matrix of the sample MS2 (10.49 wt.%Mo) aged at 480 °C for 6 h; (**a**) DF-TEM image (spot $2\bar{1}0$ of the precipitates, as indicated in red), inset: SAED pattern along [111] direction of matrix with the drawing of the crystallographic unit cells for the martensite (yellow) and the precipitate (cyan); (**b**) HRTEM image, the inset represents the FTT image of the region in the red square box.

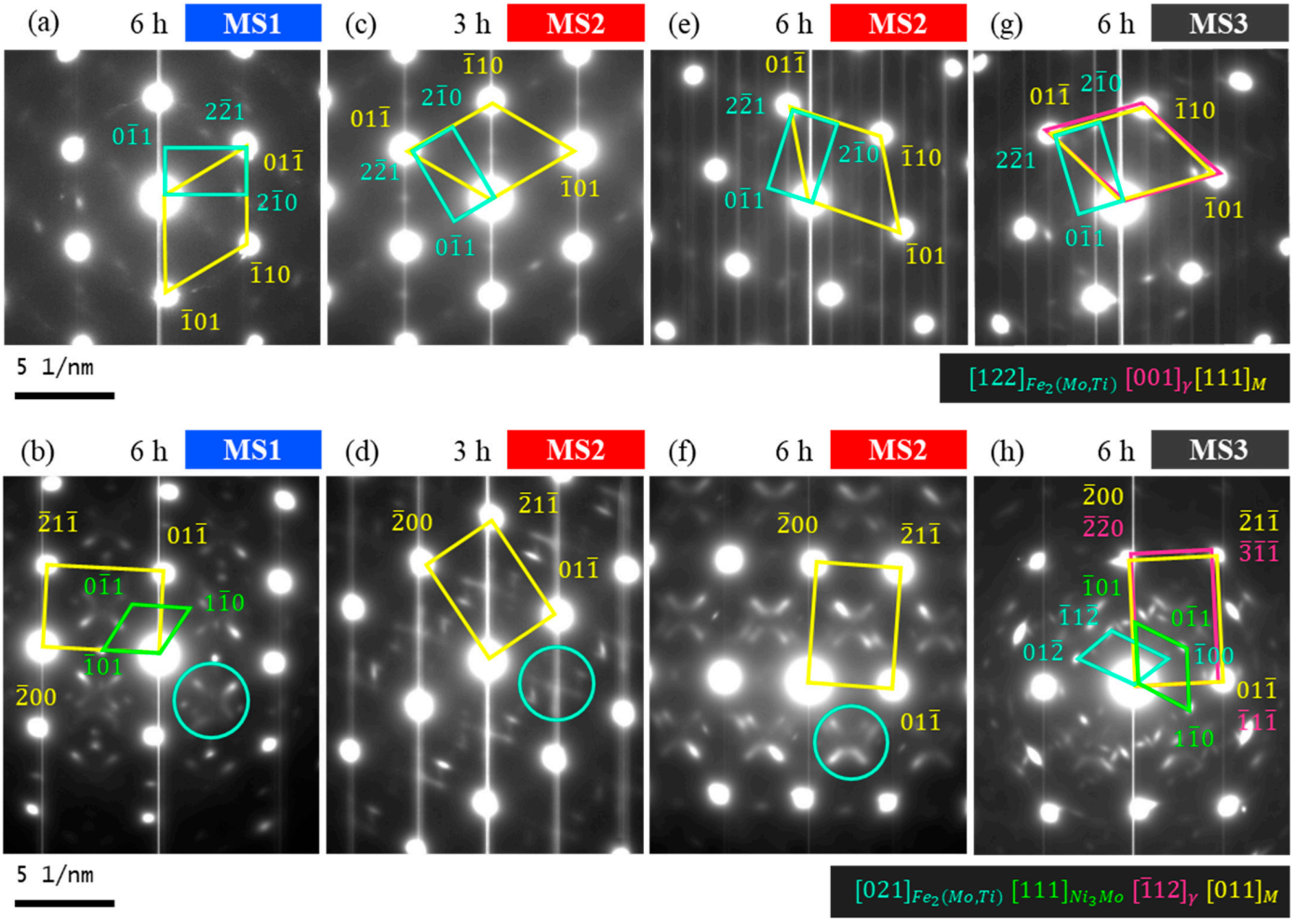


Figure 4. SAED pattern along [111] and [011] directions of matrix (**a**,**b**) MS1 (7.51wt.%Mo) aged for 6 h, (**c**,**d**) MS2 (10.49 wt.%Mo) aged for 3 h, (**e**,**f**) MS2 (10.49 wt.%Mo) aged for 6 h, and (**g**,**h**) MS3 (15.02 wt.%Mo) aged for 6 h. The unit cells of each phase are indexed as martensite in yellow, austenite in pink, $Fe_2(Mo,Ti)$ in cyan, and Ni_3Mo in green. In the bottom panels, the non-indexed phases are highlighted by cyan circles.

Table 2. Summary of the characteristics of the precipitates of each sample.

Sample	Aging Time (h)	Indexed Precipitates	Crystal Structure	Orientation Relationship p-M	Morphology [1]	Size [2]
MS1	6	Ni_3Mo	Orthorhombic	$(0\bar{1}\bar{1})_P//(\bar{1}2\bar{1})_M$ $[011]_P//[012]_M$	Spherical	Small
		Ni_3Mo	Orthorhombic	$(\bar{1}01)_P//(\bar{2}00)_M$ $[111]_P//[001]_M$	–	–
		$Fe_2(Mo,Ti)$	Hexagonal	$(0\bar{1}\bar{1})_P//(\bar{1}01)_M$ $[122]_P//[111]_M$	–	–
MS2	3	$Fe_2(Mo,Ti)$	Hexagonal	$(0\bar{1}\bar{1})_P//(\bar{1}01)_M$ $[122]_P//[111]_M$	Spherical	Small
	6	$Fe_2(Mo,Ti)$	Hexagonal	$(0\bar{1}\bar{1})_P//(\bar{1}01)_M$ $[122]_P//[111]_M$	Spherical	Small and large
MS3	6	$Fe_2(Mo,Ti)$	Hexagonal	$(\bar{1}00)_P//(\bar{2}3\bar{3})_M$ $[021]_P//[011]_M$	Spherical	Small
		Ni_3Mo	Orthorhombic	$(\bar{1}01)_P//(\bar{2}00)_M$ $[111]_P//[001]_M$	Spherical	Small and large
		$Fe_2(Mo,Ti)$	Hexagonal	$(0\bar{1}\bar{1})_P//(\bar{1}01)_M$ $[122]_P//[111]_M$	–	–

[1] Unclassified phases were indexed only using SAED, and no DF-TEM images were generated. [2] Small $\leq$ 8 nm, large > 8 nm.

In the zone axis [111] of the matrix (Figure 4a,c,e,g), a single phase was indexed for all samples (unit cell in cyan). This hexagonal phase exhibited interplanar distance values similar to those of Laves phases Fe_2Mo and Fe_2Ti. Considering that intermetallic phases form solid solutions with each other, the most suitable indexation for these precipitates would be $Fe_2(Mo,Ti)$, with a predominance of molybdenum and a smaller amount of titanium replacing molybdenum [22,32].

In the zone axis [011] of the matrix (Figure 4b,d,f,h), the indexing was more complex, and at least four patterns corresponding to precipitate phases were identified. In all samples, the presence of a non-indexed phase (identified by cyan circles) was observed, and a clear pattern among the spots of this phase could not be identified. However, it is believed that this phase may be the $Fe_2(Mo,Ti)$ phase, as it was identified in the SAEDs of the [111] zone axis (Figure 4a,c,e,g) for all samples.

Sample MS1, in addition to the $Fe_2(Mo,Ti)$ phase (circles in cyan), exhibited the Ni_3Mo orthorhombic structure phase (Figure 4b, unit cell in green), with an orientation relationship between the precipitate and matrix given by $(\bar{1}01)_P//(\bar{2}00)_M$, $[111]_P//[011]_M$.

For the MS3 sample, two phases were identified: $Fe_2(Mo,Ti)$ (Figure 4h, unit cell in cyan) and $Ni_3Mo/Ni_3(Ti,Mo)$ (Figure 4h, unit cell in green). The spots indexed for the $Fe_2(Mo,Ti)$ phase in the MS3 sample (Figure 4h in cyan) were the same spots (circles) that could not be indexed for the other samples (Figure 4b,d,f). It is believed that the spots appeared better defined in the SAED of the MS3 sample due to its higher volume fraction of precipitates of this phase. The precipitates corresponding to the second phase ($Ni_3Mo/Ni_3(Ti,Mo)$) exhibited spherical morphology, with a maximum diameter of 13.4 nm. The greater number of large particles and the coexistence of particles with varying sizes suggest that these precipitates ($Ni_3Mo/Ni_3(Ti,Mo)$) formed before the $Fe_2(Mo,Ti)$ precipitates and underwent coarsening after 6 h of aging. There is a consensus among the various authors who have worked with maraging steels that the Ni_3Ti and Ni_3Mo precipitates form before Fe_2Mo and Fe_2Ti precipitates, as they are more stable [4,9,20]. Recent

studies have also observed that Laves phases not only form after but also at the interface of Ni_3Ti and Ni_3Mo precipitates with the matrix [8,16,27]. Our results can reinforce this, since we found an orientation relationship between the Laves phase and Ni_3Mo, given by $(01\bar{2})_{Fe_2(Mo,Ti)}//(\bar{1}10)_{Ni_3Mo}$, $[021]_{Fe_2(Mo,Ti)}//[111]_{Ni_3Mo}$.

Regarding Ni_3Ti and Ni_3Mo phases, most studies on maraging steels have consistently reported the presence of Ni_3Ti in the early stages of aging and have indicated that molybdenum only begins to participate in the phase formation for longer aging times [8,16,27]. Furthermore, it is progressively established that Ni_3Ti-type precipitates exhibit needle-like morphology. However, most of these more recent works, carried out with higher resolution experimental techniques, are on steels with a higher nickel content (17–18 wt.%Ni) and a low molybdenum content (4–7 wt.%Mo) [8]. Our transmission electron microscopy results did not reveal precipitates with needle-like morphology in any of the compositions, conditions, or zone axes, even in sample MS1, which contains a lower molybdenum content (7.51 wt.%Mo), or in sample MS2, which contains a higher titanium content (0.88 wt.%Ti). Studies with alloys closer in composition to those studied here, containing 13 wt.%Ni, indicate the presence of spherical Ni_3Mo precipitates rather than Ni_3Ti [4,9,19,20]. Some studies also indicate the formation of $Ni_3(Mo,Ti)$, since the orthorhombic structure can be considered a distortion of the hexagonal lattice [12,22].

This indicates that the titanium and molybdenum content influence the type of precipitate that forms in the early stages: Ni_3Ti or Ni_3Mo. Alloys with higher titanium contents preferentially form Ni_3Ti, while alloys with higher molybdenum contents preferentially form Ni_3Mo. This is consistent with the literature, which explains why the Ni_3Ti phase is preferentially formed over Ni_3Mo, due to the higher interaction energy between nickel and titanium and the low diffusivity of molybdenum in the matrix [8,27].

In the case of MS1 and MS3 samples, which contain a lower titanium content (relative to MS2 and 18Ni maraging) and a higher molybdenum content, the formation of Ni_3Mo is favored because fewer titanium atoms are available in the matrix, and factors like the low diffusivity of molybdenum in the matrix have a lesser contribution.

While the MS1 and MS3 samples indicated the presence of Laves and Ni_3Mo phases, the MS2 sample showed no evidence of phases other than Laves. This discrepancy can be attributed to the influence of the titanium content, as the MS2 sample contains 0.88 wt.%Ti, whereas the MS1 and MS3 samples contain 0.25 wt.%Ti and 0.24 wt.%Ti, respectively. According to the literature, it is possible that in the early stages of aging of sample MS2, a phase such as Ni_3Ti, Ni_3Mo, or $Ni_3(Ti,Mo)$ formed and subsequently decomposed into the Laves phase, even before aging for 3 h. We believe the metastable phase that precedes Laves in MS2 is Ni_3Ti, as it has been consistently detected in maraging steel alloys and is consistent with the results obtained here. In samples MS1 and MS3, which formed Ni_3Mo, it remained stable even after 6 h of aging, for both higher and lower molybdenum contents. The stability of Ni_3Ti-type precipitates should be associated with the nickel content, as the works that identified the presence of Ni_3Ti even after 4 h contained nickel contents of the order of 18 wt.% [8].

Based on these assumptions and a comparison of the MS1, MS2, and MS3 samples, it is evident that the Ni_3Mo phase remains stable longer than the Ni_3Ti phase, as Ni_3Mo is still present in both MS1 and MS3 after 6 h of aging. This is consistent, as the driving force for Laves phase nucleation is the accumulation of molybdenum atoms in the vicinity of the precipitates in the early stages [8]. If the precipitates formed initially are of the Ni_3Mo type, the concentration of molybdenum remaining in the matrix will be lower, necessitating more time for diffusion and accumulation of molybdenum atoms and, consequently, later nucleation of the Laves phase. This also aligns with the observation that the Laves phase forms earlier in the MS3 sample (15.02 wt.%Mo) than in MS1 (7.51 wt.%Mo).

3.3. Precipitation Hardening

Figure 5 shows the hardness of the samples in their initial condition (AN) and after aging for 3, 4, 5, and 6 h at 480 °C. After 3 h of aging, all the samples showed a significant

increase in hardness. Over the course of 6 h of aging, the hardness of the base composition (MS2—10.49 wt.%Mo) increased by 225%, rising from 355 ± 9 HV1 to 798 ± 12 HV1. As expected, the sample with low Mo content (MS1—7.51 wt.%Mo) achieved a relatively lower maximum hardness of 681 ± 7 HV1. Conversely, the high Mo content sample (MS3—15.02 wt.%Mo) achieved a maximum hardness of 582 ± 49 HV1. However, the MS3 sample did not achieve a higher hardness due to the presence of retained austenite (RA). In the austenite regions, precipitation does not occur, because the chemical composition is not favorable and because of a lower dislocation density. Because of this, the MS3 sample will have precipitate-free regions and consequently a lower hardness. The relatively large error bars were attributed to the variations in hardness between the areas of retained austenite (RA) and the areas of aged martensite.

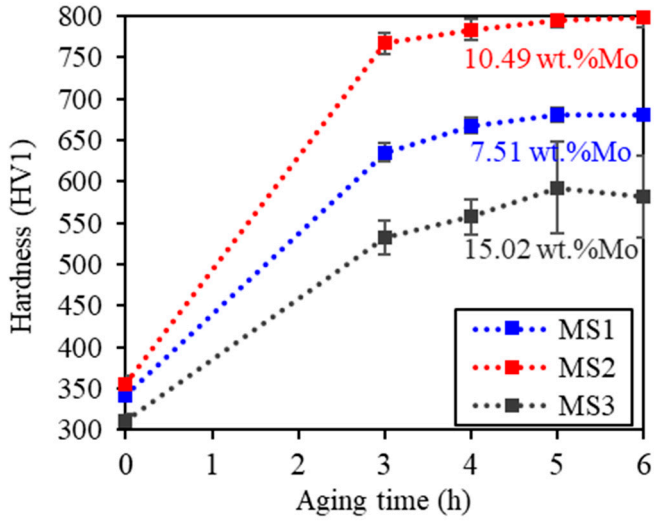


Figure 5. Vickers hardness versus aging time (480 °C) for the samples with different Mo content. Sample MS2 (base composition) was the one with the highest hardness, achieving the peak hardness close to 6 h aging. Sample MS3, containing retained austenite, was the one with the lowest hardness values and the highest error bars.

There are multiples strengthening mechanisms influencing the hardness of 13Ni maraging steels. Solid solution strengthening involves an increase in the critical resolved shear stress due to the presence of substituted solute atoms. The solid solution hardening effects from atoms like molybdenum and titanium on the matrix decrease as the volume fraction of precipitates increases [8,33]. Strengthening via a grain size reduction contributes and, in the case of maraging steels, it is associated with the packet and block sizes. Since packets and blocks are structures with high-angle boundaries, they effectively act as grains, and their dimensions have a greater influence on the strengthening mechanism through a grain size reduction than the grain size of the primary austenite [29,34]. Moreover, the strain hardening, which may result from the interaction of strain fields of high-density dislocations and dislocation tangles present in the microstructure of these steels in the annealed condition, also plays a role [33].

Although the strengthening mechanisms of the solid solution, packet sizes, and strain hardening influence the hardness of 13Ni maraging steel, during the aging, the precipitation hardening mechanisms start to dominate. At the peak hardness, precipitation hardening becomes the main strengthening mechanism. The hardness results support this; note in Figure 5 that the MS1 and MS2 samples, both containing only the martensite phase (see XRD in the Appendix A), have statistically equal hardness values before aging (342 ± 7 HV1 and 355 ± 9 HV1, respectively) and very different values after aging (681 ± 7 HV1 and 798 ± 12 HV1, respectively).

According to precipitation hardening mechanisms models, these very small precipitates, coherent and/or semi-coherent with the matrix, are sheared by the dislocation in their

slip planes during the plastic deformation of the material. This leads to a high hardness value, and the maximum value of the hardness/mechanical strength versus the aging time curve (peak hardness) occurs when the volume fraction of precipitates reaches the equilibrium value [27,35–37].

Regarding the behavior of the hardness curves of samples MS1 and MS2 (curves in blue and red), from 3 h to 4 h, the curves are still rising, followed by a gradual growth between the intervals up to 6 h. For example, considering the 3–6 h stretch, there is a growth of 7% for sample MS1 and 4% for sample MS2. Even without aging for longer times, it is possible to affirm that the peak hardness of these compositions seems to be close to 6 h, since the curves showed a tendency of stabilization after 4 h of aging.

The MS2 sample, which presented higher hardness values, was also the one that presented only Fe_2(Mo,Ti)-type precipitates. This indicates that the Laves phase can strengthen the matrix more than Ni_3Mo or Ni_3Ti. In addition, the hardness values continue to increase from 3 h to 6 h. As shown in Table 2, from 3 h to 6 h, the coarsening of Fe_2(Mo,Ti) precipitates already occurs. That is, at the peak hardness, the shear and Orowan ring hardening mechanisms are becoming active.

The results also demonstrated that it is possible that the Fe_2(Mo,Ti) precipitates are mainly responsible for the ultra-high mechanical strength of 13Ni maraging steels. The most present precipitates in 18Ni maraging steels are of the Ni_3Ti type, and these steels do not reach the high values of yield strength and ultimate tensile strength as 13Ni maraging. The ultra-high strength of 13Ni maraging steels is achieved by the combination of the precipitate type—Fe_2(Mo,Ti)—and precipitate size distribution of 3–14 nm (minimum and maximum diameter calculated for the precipitates in this sample).

4. Conclusions

The phase transformations in 13Ni maraging steels have been the subject of continuous studies since their discovery. However, there are still many gaps and discrepancies in the literature due to the complexity involved in characterizing the nanometric precipitates responsible for the high mechanical strength of these steels and due the focus of the literature on 18Ni maraging steels. In this study, microstructural characterization using HRTEM and SAED of 13Ni maraging steel samples allowed us to investigate the phase transformations in the solid-state and the precipitation hardening, leading to the following conclusions:

- 13Ni maraging steels exhibit a martensitic microstructure with pack, block, lath, and a high density of dislocations and dislocation tangles. During aging, martensite recovery occurs, involving the rearrangement of dislocations and the formation of subgrains, while precipitation took place in areas previously occupied by the dislocation tangles.
- 13Ni maraging steels containing high levels of molybdenum (15.02 wt.%Mo) may also exhibit retained austenite (RA), inside the martensite laths and at the lath boundaries.
- The type of the precipitate formed in the early stages depends on the molybdenum content and also on the nickel and titanium content. The preference is to form Ni_3Ti; however, when there are more molybdenum atoms available, it can form Ni_3Mo.
- Later than Ni_3Ti and Ni_3Mo formation, the Fe_2(Mo,Ti) Laves precipitates form, which are more stable. This phase is uniformly distributed throughout the matrix as single-crystals particles with a spherical morphology.
- Higher molybdenum contents accelerated the precipitation and coarsening kinetics of the Laves Fe_2(Mo,Ti) phase.
- The ultra-high strength of 13Ni maraging steels is achieved by the combination of the precipitate type and size distribution. The base composition of 13Ni maraging steels achieves the peak hardness by the precipitation of the Laves Fe_2(Mo,Ti) phase with a size distribution in the range of 3–14 nm.

Author Contributions: Conceptualization, D.P.M.d.F. and A.F.P.; methodology, D.P.M.d.F., E.A. and B.S.A.; software, D.P.M.d.F.; validation, D.P.M.d.F., M.V.P.A., E.A., B.S.A. and A.F.P.; formal analysis, D.P.M.d.F. and M.V.P.A.; investigation, D.P.M.d.F., M.V.P.A., E.A. and B.S.A.; resources,

M.V.P.A., B.S.A. and A.F.P.; data curation, D.P.M.d.F.; writing—original draft preparation, D.P.M.d.F.; writing—review and editing, D.P.M.d.F., M.V.P.A., E.A., B.S.A. and A.F.P.; visualization, D.P.M.d.F.; supervision, M.V.P.A. and A.F.P.; project administration, A.F.P.; funding acquisition, D.P.M.d.F., M.V.P.A. and B.S.A. All authors have read and agreed to the published version of the manuscript.

Funding: This study was financed in part by the National Council for Scientific and Technological Development (CNPq)—grant number 168256/2018-5—and by the Coordenação de Aperfeiçoamento de Pessoal de Nível Superior—Brasil (CAPES)—Finance Code 88887.570306/2020-00.

Data Availability Statement: Data are contained within the article.

Acknowledgments: Work at the Molecular Foundry was supported by the Office of Science, Office of Basic Energy Sciences, of the U.S. Department of Energy under Contract No. DE-AC02-05CH11231. The authors would like to acknowledge the National Institute of Metrology, Standardization and Industrial Quality (INMETRO).

Conflicts of Interest: The authors declare no conflict of interest.

Appendix A

Figure A1 presents the X-ray diffractograms of the samples MS1, MS2, and MS3 annealed at 1200 °C for 1 h. The results were obtained using a Philips X'Pert-MPD diffractometer with CuKα radiation (λ = 1.5418 Å), $20° \leq 2\theta \leq 100°$, $\Delta 2\theta = 0.02°$, and $\Delta t = 200$ s.

The three diffractograms exhibited peaks corresponding to the matrix phase—Fe-α′ martensite (CCC structure)—as indicated by solid lines. Sample MS3 also exhibited peaks corresponding to austenite—Fe-γ (FCC structure)—indicated by dashed lines. This austenite is referred to in the literature as retained austenite. As it was detected in the annealed material, it can be stated that this austenite forms during the annealing process, and after quenching, it did not transform completely into martensite. Instead, it remained stable even at room temperature due to factors such as composition, cooling rate, and cooling temperature [38,39].

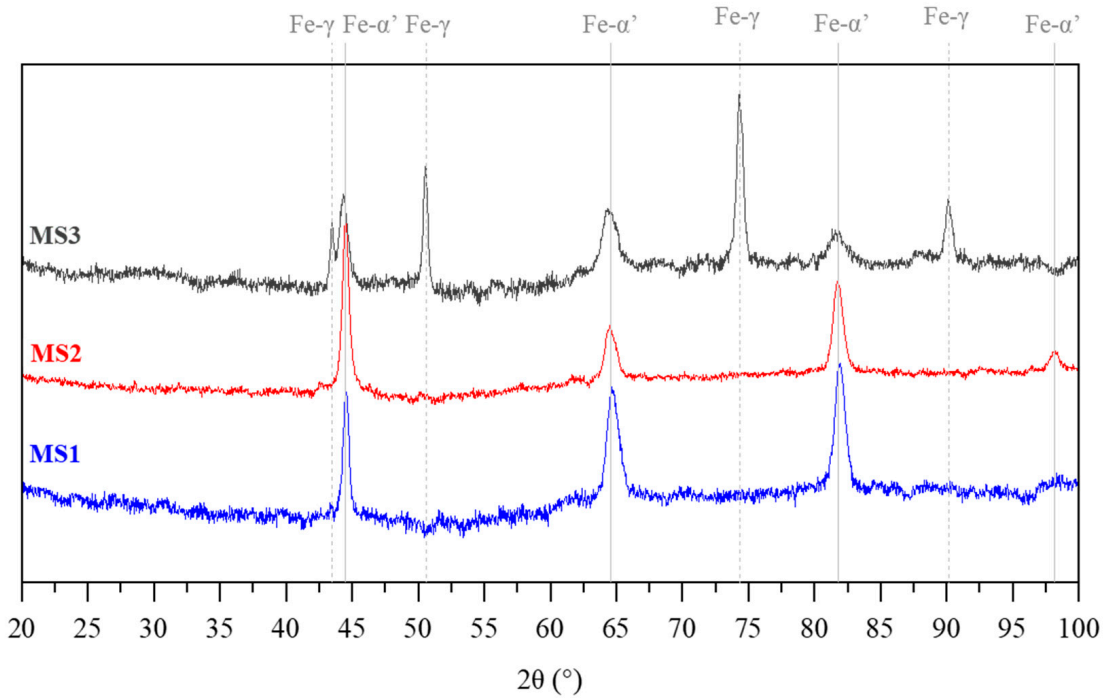


Figure A1. X-ray diffractograms with CuKα radiation (λ = 1.5418 Å) of samples MS1 (blue), MS2 (red), and MS3 (dark grey) annealed at 1200 °C for 1h, showing peaks of ferrite (continuous lines) and austenite phases (dotted lines).

References

1. Hornbogen, E.; Rittner, K. Development of Thermo-Mechanical Treatments of a Maraging Steel for Yield Strengths above 3 GPa. *Steel Res.* **1987**, *58*, 172–177. [CrossRef]
2. Schmidt, M.; Rohrbach, K. Heat Treatment of Maraging Steels. In *ASM Handbook—VOLUME 4: Heat Treating*; ASM International: Phoenix, AZ, USA, 1991; pp. 528–548.
3. Sha, W.; Guo, Z. *Maraging Steels: Modelling of Microstructure, Properties and Applications*; Woodhead Publishing Limited: New York, NY, USA, 2009; ISBN 9781845693756.
4. Maganée, A.; Drapier, J.M.; Dumont, J.; Coutsouradis, D.; Habraken, L. *Cobalt Monograph Series—Cobalt-Containing High-Strength Steels: A Critical Review of the Physical Metallurgy of Cobaltcontaining High-Strength Steels, and a Survey of Their Processing, Properties and Uses*; Centre D'Information du Cobalt: Brussels, Belgium, 1974.
5. Pereloma, E.; Edmonds, D.V. *Phase Transformations in Steels-Volume 2: Diffusionless Transformations, High Strength Steels, Modelling and Advanced Analytical Techniques*; Woodhead Publishing Limited: Cambridge, UK, 2012; ISBN 978-0-85709-611-1. (online).
6. He, Y.; Yang, K.; Sha, W. Transmission Electron Microscopy of New High-Strength Grade Maraging Steels. *Microsc. Anal.* **2007**, *21*, 5–7.
7. Wang, W.; Yan, W.; Duan, Q.; Shan, Y.; Zhang, Z.; Yang, K. Study on Fatigue Property of a New 2.8GPa Grade Maraging Steel. *Mater. Sci. Eng. A* **2010**, *527*, 3057–3063. [CrossRef]
8. Niu, M.; Zhou, G.; Wang, W.; Shahzad, M.B.; Shan, Y.; Yang, K. Precipitate Evolution and Strengthening Behavior during Aging Process in a 2.5 GPa Grade Maraging Steel. *Acta Mater.* **2019**, *179*, 296–307. [CrossRef]
9. Menzel, J.; Klaar, H.-J. Systematische Gefiigeuntersuchungen Am Martensitaushirtenden Stahl X 2 NiCoMo 13 15 10. *Steel Res.* **1990**, *61*, 30–38. [CrossRef]
10. De Carvalho, L.G.; Plaut, R.L.; Padilha, A.F. Precipitation Kinetic Analysis in a Maraging 350 Steel Using KJMA and Austin-Rickett Equations. *Defect Diffus. Forum* **2022**, *420*, 118–128. [CrossRef]
11. De Carvalho, L.G.; Plaut, R.L.; de Lima, N.B.; Padilha, A.F. Kinetics of Martensite Reversion to Austenite during Overaging in a Maraging 350 Steel. *ISIJ Int.* **2019**, *59*, 1119–1127. [CrossRef]
12. Tian, J.; Wang, W.; Li, H.; Shahzad, M.B.; Shan, Y.; Jiang, Z.; Yang, K. Effect of Deformation on Precipitation Hardening Behavior of a Maraging Steel in the Aging Process. *Mater. Charact.* **2019**, *155*, 109827. [CrossRef]
13. Truong, T.D.; Asala, G.; Ola, O.T.; Ojo, O.A.; Odeshi, A.G. Texture and Damage Evolution in Additively Manufactured 18%Ni-M350 Maraging Steel under Dynamic Impact Loading: Processing Parameters and Heat Treatment Effects. *Materialia* **2023**, *32*, 101961. [CrossRef]
14. Zeisl, S.; Van Steenberge, N.; Schnitzer, R. Strengthening Effect of NiAl and Ni3Ti Precipitates in Co-Free Maraging Steels. *J. Mater. Sci.* **2023**, *58*, 7149–7160. [CrossRef]
15. Patil, V.V.; Mohanty, C.P.; Prashanth, K.G. Selective Laser Melting of a Novel 13Ni400 Maraging Steel: Material Characterization and Process Optimization. *J. Mater. Res. Technol.* **2023**, *27*, 3979–3995. [CrossRef]
16. Niu, M.C.; Yin, L.C.; Yang, K.; Luan, J.H.; Wang, W.; Jiao, Z.B. Synergistic Alloying Effects on Nanoscale Precipitation and Mechanical Properties of Ultrahigh-Strength Steels Strengthened by Ni_3Ti, Mo-Enriched, and Cr-Rich Co-Precipitates. *Acta Mater.* **2021**, *209*, 116788. [CrossRef]
17. Tian, J.; Wang, W.; Babar Shahzad, M.; Yan, W.; Shan, Y.; Jiang, Z.; Yang, K. A New Maraging Stainless Steel with Excellent Strength–Toughness–Corrosion Synergy. *Materials* **2017**, *10*, 1293. [CrossRef]
18. Bourgeot, J.; Maitrepierre, P.; Manenc, J.; Thomas, B. Hardening Fe-Ni-Mo and Fe-Ni-Co-Mo Martensitic Alloys by Tempering. *IRSID Int. Rep. No 116* **1971**.
19. Fukamachi, M.; Kawabe, Y.; Nakazawa, K.; Muneki, S. Transmission Electron Microscopy Studies of Structural Changes in 13Ni-15Co-10Mo Maraging Steel as a Result of Aging. *J. Japan Inst. Metals* **1983**, *47*, 237–242. [CrossRef]
20. Floreen, S. The Physical Metallurgy of Maraging Steels. *Metall. Rev.* **1968**, *13*, 115–128. [CrossRef]
21. Niu, M.C.; Chen, C.J.; Li, W.; Yang, K.; Luan, J.H.; Wang, W.; Jiao, Z.B. Atomic-Scale Understanding of Solute Interaction Effects on Grain Boundary Segregation, Precipitation, and Fracture of Ultrahigh-Strength Maraging Steels. *Acta Mater.* **2023**, *253*, 118972. [CrossRef]
22. Viswanathan, U.K.; Dey, G.K.; Asundi, M.K. Precipitation Hardening in 350 Grade Maraging Steel. *Metall. Trans. A* **1993**, *24*, 2429–2442. [CrossRef]
23. Vasudevan, V.K.; Kim, S.J.; Wayman, C.M. Precipitation Reactions and Strengthening Behavior in 18 Wt Pct Nickel Maraging Steels. *Metall. Trans. A* **1990**, *21A*, 2655–2668. [CrossRef]
24. Da Fonseca, D.P.M.; de Carvalho, L.G.; de Lima, N.B.; Padilha, A.F. Austenite Formation in the Oxidized Layer of Ultra-High-Strength 13Ni15Co10Mo Maraging Steel. *Metals* **2022**, *12*, 2115. [CrossRef]
25. Porter, D.A.; Easterling, K.E.; Sherif, M.Y. *Phase Transformations in Metals and Alloys*, 3rd ed.; CRC Press: Boca Raton, FL, USA, 2009; Volume 59, ISBN 9781439883570.
26. Krauss, G. Solidification, Segregation, and Banding in Carbon and Alloy Steels. *Metall. Mater. Trans. B* **2003**, *34*, 781–792. [CrossRef]
27. Fang, J.Y.C.; Liu, W.H.; Yang, T.; Wu, Y.; Jiao, Z.B. Multicomponent Precipitation and Strengthening in Intermetallic-Strengthened Alloys. *Front. Mater.* **2022**, *9*, 2–7. [CrossRef]

28. Feitosa, A.L.M.; Escobar, J.; Ribamar, G.G.; Avila, J.A.; Padilha, A.F. Direct Observation of Austenite Reversion During Aging of 18Ni (350 Grade) Maraging Steel Through In-Situ Synchrotron X-ray Diffraction. *Metall. Mater. Trans. A* **2022**, *53*, 420–431. [CrossRef]
29. Morito, S.; Huang, X.; Furuhara, T.; Maki, T.; Hansen, N. The Morphology and Crystallography of Lath Martensite in Alloy Steels. *Acta Mater.* **2006**, *54*, 5323–5331. [CrossRef]
30. Morito, S.; Tanaka, H.; Konishi, R.; Furuhara, T.; Maki, T. The Morphology and Crystallography of Lath Martensite in Fe-C Alloys. *Acta Mater.* **2003**, *51*, 1789–1799. [CrossRef]
31. Morito, S.; Saito, H.; Ogawa, T.; Furuhara, T.; Maki, T. Effect of Austenite Grain Size on the Morphology and Crystallog- Raphy of Lath Martensite in Low Carbon Steels. *ISIJ Int.* **2005**, *45*, 91–94. [CrossRef]
32. Raghavan, V. Fe-Mo-Ti (Iron-Molybdenum-Titanium). *J. Phase Equilibria* **2003**, *24*, 182–183. [CrossRef]
33. Argon, A.S. *Strengthening Mechanisms in Crystal Plasticity*; Oxford University Press: Oxford, UK, 2008.
34. Maki, T.; Tsuzaki, K.; Tamura, I. The Morphology of Microstructure Composed of Lath Martensites in Steels. *Trans. Iron Steel Inst. Jpn.* **1980**, *20*, 207–214. [CrossRef]
35. Blankenship, C.P.; Hornbogen, E.; Starke, E.A. Predicting Slip Behavior in Alloys Containing Shearable and Strong Particles. *Mater. Sci. Eng. A* **1993**, *169*, 33–41. [CrossRef]
36. Meyers, M.A.; Chawla, K.K. *Mechanical Behavior of Materials*, 2nd ed.; Cambridge University Press: New York, NY, USA, 2008; ISBN 9780521866750.
37. Peng, S.; Wang, Z.; Li, J.; Fang, Q.; Wei, Y. Beyond Orowan Hardening: Mapping the Four Distinct Mechanisms Associated with Dislocation-Precipitate Interaction. *Int. J. Plast.* **2023**, *169*, 103710. [CrossRef]
38. Berns, H.; Theisen, W. *Ferrous Materials: Steel and Cast Iron*; Springer: Berlin/Heidelberg, Germany, 2008; Volume 53, ISBN 9783540718475.
39. Hossain, R.; Pahlevani, F.; Quadir, M.Z.; Sahajwalla, V. Stability of Retained Austenite in High Carbon Steel under Compressive Stress: An Investigation from Macro to Nano Scale. *Sci. Rep.* **2016**, *6*, 34958. [CrossRef]

Disclaimer/Publisher's Note: The statements, opinions and data contained in all publications are solely those of the individual author(s) and contributor(s) and not of MDPI and/or the editor(s). MDPI and/or the editor(s) disclaim responsibility for any injury to people or property resulting from any ideas, methods, instructions or products referred to in the content.